Journal of Inorganic Biochemistry 201 (2019) 110807

Contents lists available at ScienceDirect

Journal of Inorganic Biochemistry

journal homepage: www.elsevier.com/locate/jinorgbio

Assembly behavior of amylin fragment hIAPP19-37 regulated by Au(III) complexes

Xiangyi Huang, Jufei Xu, Weihong Du*

Department of Chemistry, Renmin University of China, Beijing 100872, China

ARTICLE INFO

Keywords:
Au(III) complex
hIAPP19-37
Aggregation
Interaction
Inhibition

ABSTRACT

Human islet amyloid polypeptide (hIAPP, amylin) may self-aggregate and rupture the membrane of β cells, which is closely correlated with the pathogenesis of type 2 diabetes mellitus (T2DM). Hence, suppressing amyloidogenic hIAPP may be beneficial for the treatment of diabetes. As an important part of hIAPP, the fragment hIAPP19-37 was studied in this work to explore their disaggregation and cellular behavior regulation by some selected Au complexes, as follows: dichloro diethyl dithiocarbamate Au complex [$AuCl_2$(DDTC)] (**1**), dichloro pyrrolidine dithiocarbamate Au complex [$AuCl_2$(PDT)] (**2**), dichloro 4-4′-dimethyl-2,2′-bipyridyl Au (III) chloride [$AuCl_2(Me)_2$bpy]Cl (**3**), and dichloro 4-4-di-tert-butyl-2,2′-bipyridyl Au(III) chloride [$AuCl_2$(t-Bu)$_2$bpy]Cl (**4**). The peptide aggregation was observed and analyzed by fluorescence assay, atomic force microscopy (AFM), dynamic light scattering (DLS) and other methods. The assembly behaviors of hIAPP19-37 affected by the four Au complexes indicated that these complexes could effectively inhibit the fibrillation of the peptide and depolymerized the aged peptide into nanoscale particles. These Au compounds also remarkably reduced membrane leakage and cytotoxicity caused by peptide oligomers. An interaction study revealed that the complexes were predominantly bound with hIAPP19-37 through hydrophobic and electrostatic interactions, and metal coordination. The differences among various complexes were compared according to their binding affinity, inhibitory effect, and cellular behavior. Our study offers a potential path for the possible utilization of Au compounds as amyloidosis inhibitors.

1. Introduction

The amyloid deposition of some proteins and peptides are associated with a series of diseases, such as α-synuclein with Parkinson's disease, amyloid-β protein (Aβ) and tau protein with Alzheimer's disease, and human islet amyloid polypeptide with T2DM [1,2]. hIAPP consists of 37 amino acids and is co-secreted with insulin by β-cells [3,4]. The hIAPP fragment hIAPP19-37 (SSNNFGAILSSTNVGSNTY-NH_2) is an important component of the full peptide hIAPP1-37. The differences in the species-specific amino acid sequence of IAPP mainly focus on the sequence 20-29. Compared with the fragment of nonamyloidogenic rat amylin rat-IAPP20-29, hIAPP20-29 has a tendency to spontaneously aggregate. Moreover, there are three aromatic residues in the sequence of hIAPP, two of them are located in the fragment hIAPP19-37, phenylalanine 23 (Phe23) and tyrosine 37 (Tyr37). These aromatic residues may interact with each other and with aromatic compounds by π–π stacking. It has been reported that Phe-Phe interaction within the hydrophobic core make the fibers more stable. Therefore, the fragment hIAPP19-37 acts as a key regulatory sequence to produce amyloidosis [5–9].

Inhibitors of amylin deposition have been extensively studied. Many small organic molecules, natural products, and metal compounds affect the aggregation and depolymerization of amylin through hydrophobic and electrostatic interactions and hydrogen bonding [9–12]. Metals and their complexes, such as the anticancer cisplatin, the anti-inflammatory auranofin, and masses of metal diagnostic reagents, are widely utilized for disease treatment and demonstrate diverse biological functions [13–19]. Metal ions can interact with amylin and have a favorable effect on the speed, strength, and morphology of amylin aggregation [15,20]. Zn(II) ions may resist hIAPP aggregation at low concentration, but they increase hIAPP aggregation at high concentration [15]. Given their advantages of distinct metal center and ligand with different configurations, ruthenium complexes have become potential inhibitors of amyloidosis [21,22]. Au has been widely used for the treatment of various diseases since the ancient times. Au(III), Au(I) compounds, and Au nanoparticles exhibit good antibacterial, antitumor, and anti-amyloidosis activities [23–28]. For example, Au complexes may inhibit hIAPP aggregation and the prion protein (PrP) neuropeptide PrP106-

* Corresponding author.
E-mail address: whdu@ruc.edu.cn (W. Du).

https://doi.org/10.1016/j.jinorgbio.2019.110807
Received 14 June 2019; Received in revised form 3 August 2019; Accepted 23 August 2019
Available online 29 August 2019
0162-0134/

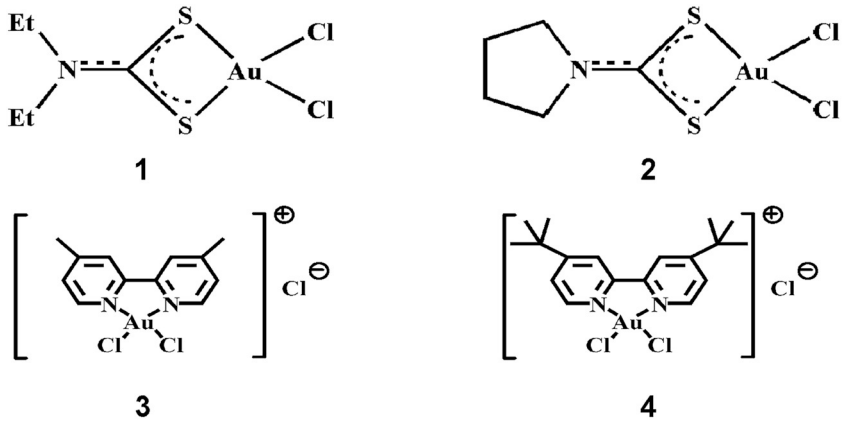

Scheme 1. Molecular structures of Au complexes [$AuCl_2$(DDTC)] (**1**), [$AuCl_2$(PDT)] (**2**), [Au(Me_2bpy)Cl_2]Cl (**3**), [Au(t-Bu_2bpy)Cl_2]Cl (**4**).

126 via metal coordination as a major binding force. The compound [Au(bipy)Cl_2][PF_6] regulates hIAPP aggregation through a dimer transient state [29]. However, the effects of Au center and ligand configuration on the assembly behavior and binding affinity of different peptides remain obscure and need further exploration.

In this study, we synthesized four Au complexes (Scheme 1), dichloro diethyl dithiocarbamate Au complex [$AuCl_2$(DDTC)] (**1**), dichloro pyrrolidine dithiocarbamate Au complex [$AuCl_2$(PDT)] (**2**), dichloro 4-4′-dimethyl-2,2′-bipyridyl Au(III) chloride [$AuCl_2$($Me)_2$bpy]Cl (**3**), dichloro 4-4-di-tert-butyl-2,2′-bipyridyl Au(III) chloride [$AuCl_2$(t-$Bu)_2$bpy]Cl (**4**), and studied their inhibition on the aggregation of the hIAPP core fragment hIAPP19-37. We aimed to further understand the effect of Au complexes on hIAPP. We also explored the interaction mechanism between the peptide and Au complexes. Although many metal ions and metal complexes affect the peptides' amyloidosis, the effects are twofold, the inhibition or the promotion on peptide aggregation. Gold complexes better inhibit the aggregation of amyloid peptides mainly by metal coordination. Researches also find that some small aromatic organic molecules may inhibit the aggregation and depolymerize the mature amyloid fibrils through hydrophobic and electrostatic interactions. Therefore, considering Au(III) ion which provides good metal coordination, and small organic molecules which provide effective ligands to modify the complex's steric configuration, we chose the four tetra-coordinated Au(III) complexes with different ligand features. These complexes possibly possess favorable conformation advantages as amyloid inhibitors and may show good prospects for biological utilization [30–35]. We employed the thioflavin T (ThT) fluorescence assay, AFM, DLS to detect the effects of Au complexes on hIAPP19-37 aggregation and the depolymerization of the aged peptide aggregates. The intrinsic fluorescence method and electrospray ionization mass spectrometry (ESI-MS) were performed to elucidate the binding affinity of the complexes with hIAPP19-37. Furthermore, liposomal experiments, cell viability determination, and antibody immune analysis were conducted to reveal the influence of these Au complexes on the cellular behaviors of hIAPP19-37 and compare them with other reported metal compounds.

2. Experimental section

2.1. Materials

The sample hIAPP19-37 was chemically synthesized by SynPeptide Co., Ltd. (Shanghai, China). It had > 95% purity and was identified by high-performance liquid chromatography and ESI-MS. hIAPP19–37 was treated with hexafluoroisopropanol before use.

Complexes **1**, **2**, **3**, and **4** were synthetized in accordance with previous reports [36,37]. The ligands diethyl dithiocarbamate (DDTC), pyrrolidine dithiocarbamate (PDT), and 4-4′-dimethyl-2,2′-bipyridyl (($Me)_2$bpy), 4-4′-di-tert-butyl-2,2′-bipyridyl (($t-Bu)_2$bpy) were purchased from SCR Beijing Co., Ltd. (China). The liposomes 1,2-dioleoyl-sn-glycero-3-phospho-rac-(1-glycerol) sodium salt (DOPG, ≥99%) and 1,2-dioleoyl-sn-glycero-3-phosphocholine (DOPC, ≥99%) were purchased from AVT (Shanghai, China). 3-(4,5-Dimethyl-2-thiazolyl)-2,5-diphenyltetrazolium bromide (MTT) was purchased from Sigma. A11 anti-amylin antibody was obtained from the Shanghai Hao Test Biotechnology Co., Ltd. All other reagents were of analytical grade.

2.2. ThT assay

The dye ThT was used to detect the aggregation extent of hIAPP19-37 and the inhibitory effects of Au complexes on amyloid peptide deposition. hIAPP19-37 at 100 μM was dissolved in 10 mM phosphate buffer saline (PBS, pH 7.4) containing 10% dimethyl sulfoxide (DMSO). The peptide was then incubated with Au complexes at different doses at 310 K for 72 h. After 72 h of cultivation, ThT was added into these samples at a final concentration of 10 μM. The final concentration of these Au complexes was 10, 30, and 50 μM. The peptide concentration was 10 μM in solution. F-4600 (Hitachi, Ltd., Japan) was applied to detect fluorescence at 310 K. The samples were excited at 432 nm, and their fluorescent signals were received at the emission wavelength of 485 nm at a time interval of 10 s. The data were expressed as the average value of three reported spectra.

The ThT assay was also used to observe the disaggregation extent of hIAPP19-37 induced by Au complexes. Approximately 100 μM of hIAPP19-37 was dissolved in 10 mM PBS containing 10% DMSO. Subsequently, the solution was incubated at 310 K for 72 h. After 3 days, different doses of Au complexes were added to the hIAPP19-37. The mixtures were then further incubated for 72 h before detection. The final concentrations and settings of the instrument were the same as those mentioned above in the inhibition experiments.

2.3. Ultraviolet-visible (UV–vis) spectroscopy

The absorption spectra were recorded on a Cary 50 UV-Vis spectrophotometer (Agilent, USA) at room temperature to clarify the possible influence of the Au complex on ThT. The concentration of ThT used was 50 μM, and those of the Au complex were 0, 25, and 50 μM.

2.4. AFM images

AFM was used to observe the morphology of hIAPP19-37 in the inhibition, disaggregation, and time-dependent dynamics experiments. For the inhibition experiments, 100 μM of hIAPP19-37 was incubated for 72 h at 310 K in the absence and presence of Au complexes at different concentrations. The final test concentration of hIAPP19-37 was 10 μM. For Au complexes, the concentrations were 10 and 100 μM. For

the disaggregation experiments, 100 μM of hIAPP19-37 was incubated for 72 h at 310 K. Afterward, different amounts of Au complexes were mixed with hIAPP19-37, and the samples were incubated for 72 h. The samples were diluted to the same concentration as in the inhibition experiments before determination. For the time-dependent dynamics experiments, different mixture solutions containing 10 μM of hIAPP19-37 in the absence and presence of 10 and 100 μM Au complexes were incubated together and analyzed at 0, 12, and 24 h at 310 K. "Tapping in air" mode was selected with a silicon tip. The scanning rate was 1 Hz, and the scanning line was 256. The final AFM images were obtained from three repetitions.

2.5. DLS measurements

The particle size of peptide aggregates was measured by the Zetasizer Nano instrument (Malvern Instruments, Worcestershire, UK). HIAPP19-37 was incubated with different amounts of Au complexes for 72 h at 310 K. The final concentration of hIAPP19-37 was 10 μM, and the molar ratios of Au complexes to hIAPP19-37 were 0, 1, 3, and 5 respectively. The sample for the disaggregation experiment was the same as the sample preparation for the disaggregation in AFM experiments. These samples were centrifuged for 10 min at 10,000 revolution per minute to remove oversized granules. The reported value was acquired from three measurements.

2.6. Spectrofluorometric measurements

Changes in the intrinsic fluorescence of peptide and protein are extensively used to detect the interaction of a small molecule with a protein or peptide [7,38]. In this study, the residue Tyr37 of hIAPP19-37 was excited at 275 nm, and the apparent dissociation constant (K_d) was calculated from the intrinsic fluorescence change by using Formula (1),

$$\Delta F = F_0 - F_L = (F_0 - F_\alpha) \times \{K_d + P_0 + T - [(K_d + P_0 + T)^2 - 4P_0T]^{1/2}\}/2P_0 \quad (1)$$

where F_L and F_0 indicate the fluorescence intensity at 303 nm with and without the Au compounds, respectively. F_α represents the fluorescence intensity at which the protein reaches maximum quenching, P_0 is the initial concentration of the peptide, and T represents the added complex concentrations ranging from 0 to 10 μM. The experiments were performed in triplicate.

2.7. ESI-MS

The ESI-MS spectrum was recorded in positive mode at a flow rate of 3 μL min^{-1} by an APEX IV FT-ICR high resolution mass spectrometer (Bruker, USA). The peptide was dissolved directly in water and mixed with Au complex containing 10% DMSO. The solution pH was at 5.4 approximately. The final concentration used in the experiments was 50 μM for the peptide. The molar ratio of Au complex to the peptide was 5 for complexes **1** and **2** and 10 for complexes **3** and **4**.

2.8. Membrane leakage assay

Large unilamellar vesicles (LUVs) were prepared at a DOPC/DOPG liposome ratio of 7:3 to mimic the cell membranes in the membrane leakage experiments. The peptide hIAPP19-37 was added into a mixture of calcein containing 100 μM LUVs in 10 mM PBS as the control group. Five equivalent amounts of Au complexes were added into the hIAPP19-37. The final concentrations of hIAPP19-37 and Au complex were 20 and 100 μM, respectively. Fluorescence was reported by the F-4500 fluorescence spectrometer (Hitachi, Japan). The excitation wavelength was set at 485 nm, and data were recorded at an emission wavelength of 535 nm. The fluorescence was detected per hour. At the end of each test, 1 μL of 10% Triton X-100 was added to the sample to mark the maximum leakage of each measurement. The following formula was applied to calculate the amount of fluorescent dye leakage [39],

$$L(t) = (F_t - F_0)/(F_{100} - F_0) \quad (2)$$

where L (t) is the normalized membrane leakage, F_t is the fluorescence intensity measured each time, F_0 is the fluorescence intensity at $t = 0$, and F_{100} is the fluorescence intensity measured after Triton X-100 addition.

2.9. Immune assay

The peptide hIAPP19-37 was freshly dissolved in 10% DMSO-PBS at a final concentration of 100 μM in combination with Au complexes at concentrations of 0, 100, and 500 μM. Equal amounts of Au complexes at 100 and 500 μM were prepared as controls. These samples and oligomer-specific anti-amylin antibody (A11 antibody) [40] were spotted in the enzyme linked immunosorbent assay (ELISA) test plate and then coated with 0.05 M coating buffer (pH 9.6) overnight at 4 °C. After coating, the plate was washed with 0.01 M PBS–0.001% Tween 20 (pH 7.2–7.4) three times. The coated ELISA plate was blocked with 2% bovine serum albumin (BSA) blocking buffer and incubated at 37 °C for 2 h. The A11 antibody was diluted 1:1000 with 1% BSA, added to the ELISA plate at 100 μL per well, and incubated at 37 °C for 1 h. Goat anti-rabbit antibody was diluted 1:10,000 with 1% BSA, added to the ELISA plate at 100 μL per well, and incubated at 37 °C for 1 h. The sample was treated with 3,3′,5,5′ tetramethyl benzidine colorimetric kit at 25 °C for 8 min. Color number was read with a microplate reader at a wavelength of 450 nm. This experiment was performed in triplicate and the results were analyzed by one-way Analysis of Variance (ANOVA). The asterisk labeled those results which significantly differed from that of hIAPP19-37 alone.

2.10. Cell culture and MTT assay

Cell viability in the presence of hIAPP19-37 and Au compounds was determined by MTT assay. Insulinoma β cells in rat (INS-1 cells) were purchased from Bogoo Biotech Co., Ltd. (Shanghai, China). The cells were cultured in monolayer cultures on Roswell Park Memorial Institute-1640 medium supplemented with 10% fetal bovine serum, 2 mM L-glutamine, 100 U mL^{-1} penicillin, and 100 U mL^{-1} streptomycin. The INS-1 cells were incubated for 24 h at 310 K and then cultured with or without hIAPP19-37 and Au complexes. The INS-1 cells were mixed with 10 μL of MTT, and the mixture was incubated for 48 h and then at 310 K for 4 h. The final concentration of hIAPP19-37 was 15 μM. The Au complexes' concentrations were 1.5 and 15 μM. A UV–vis spectrophotometer was used to determine the absorbance of these samples at 570 nm. The results were analyzed by one-way ANOVA as well.

3. Results

3.1. Synthesis of Au complexes

Au complexes **1**, **2**, **3**, and **4** were synthetized and identified as previously described [36,37]. The UV–vis spectra of these complexes are shown in Fig. S1. The NMR and IR results (data not shown) identified that the products were consistent with the literature and could be used for further experiments.

3.2. Influence of Au complexes on hIAPP19-37 aggregation

The dye ThT can bind the peptide aggregates and show intense fluorescent emission peak at 485 nm [41]. Changes in the ThT fluorescence intensity were used to reflect the degree of hIAPP19-37 fibrillation both in the inhibition and disaggregation experiments (Figs. 1 and S2). The highest fluorescence intensity in the spectra was recorded from the aggregated peptide alone. In the presence of Au complexes, the

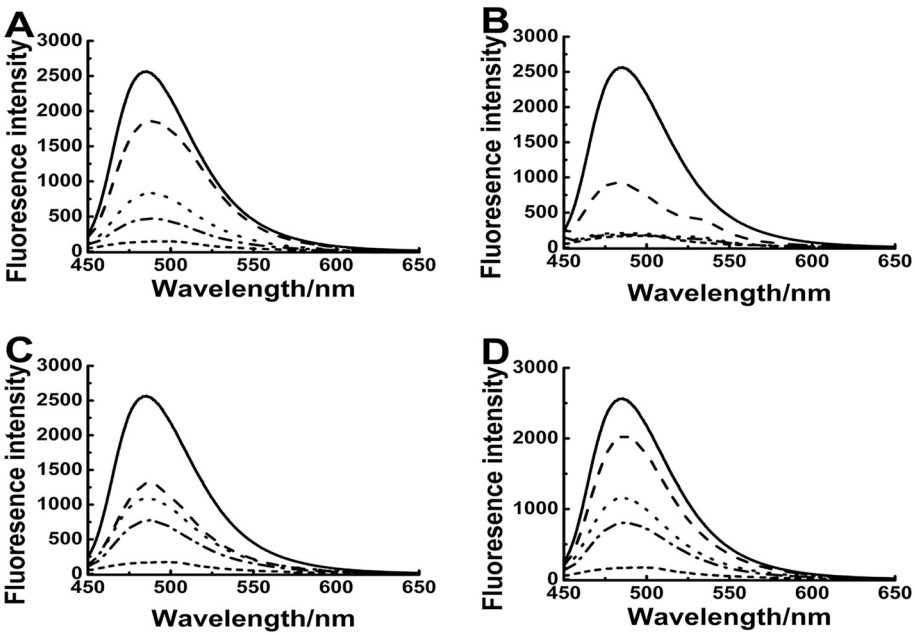

Fig. 1. ThT assay for the peptide hIAPP19-37 aggregation in the absence (solid) and presence of different concentrations of **1** (A), **2** (B), **3** (C) and **4** (D). The concentration of peptide was 10 μM. The different concentrations of Au complexes were 10 (dashed), 30 (dotted), and 50 μM (dash dotted). The concentration of ThT (short dashed) was 10 μM.

intensity of ThT fluorescence decreased gradually. The effects of the four Au complexes on hIAPP19-37 aggregation were concentration dependent, thereby reflecting that fibril formation was well-suppressed. Within the concentration range used for measurement, the fluorescence intensity decreased with increasing complex concentration. By comparison, complex **2** exhibited relatively strong inhibition and depolymerization ability against hIAPP19-37 amyloid deposition.

To clarify the interaction of ThT and metal complex, we designed a series of experiments. As suggested in Fig. S3, no clear interaction occurred among complexes **1**, **2**, and **4** and ThT. For complex **3**, when the concentration of the Au complex increased to 50 μM, the peak absorption at 418 nm was distinctly decreased, thereby implying a possible interaction existing between complex **3** and hIAPP19-37. This result indicated the disturbance of ThT by complex **3** binding to the peptide in the ThT assay. Therefore, imaging experiments were conducted to clarify the effects of metal complexes on hIAPP19-37 fibril formation.

3.3. Morphological analysis

Although ThT assay revealed inhibitory effects of Au complexes on hIAPP19-37 aggregation at certain extent, AFM can intuitively exhibit the morphological changes of hIAPP19-37 induced by Au complexes without the disturbance of other substances. Figs. 2, 3, and S4 show the AFM images for the inhibition, disaggregation, and time-dependent aggregation experiments, respectively. When hIAPP19-37 was cultured alone at 310 K for 72 h, dense fibers were observed (Fig. 2). In the presence of equivalent amounts of Au complexes, these fibers were shortened, and some spherical particles appeared. When the molar ratio of Au complex to hIAPP19-37 increased to 10, those fibrils disappeared, and the quantity of spherical particles decreased. The heights of the marked fibrils and spherical particles, which represented the average value of the aggregates in each image, were measured and presented. The heights from line a to j were 6.38, 24.28, 13.08, 19.25, 4.74, 47.24, 26.01, 23.46, 15.57 nm respectively. These values illustrate the difference between fibrous substance and globular substance [12,22], thereby indicating the effects of Au compounds on peptide aggregation.

Fig. S4 shows the results of peptide disaggregation affected by Au complexes. After incubation with equivalent amounts of Au complexes, the peptide fibrils faded away, and spherical particles arose. In the presence of complex **3**, some fibrils remained observable under the

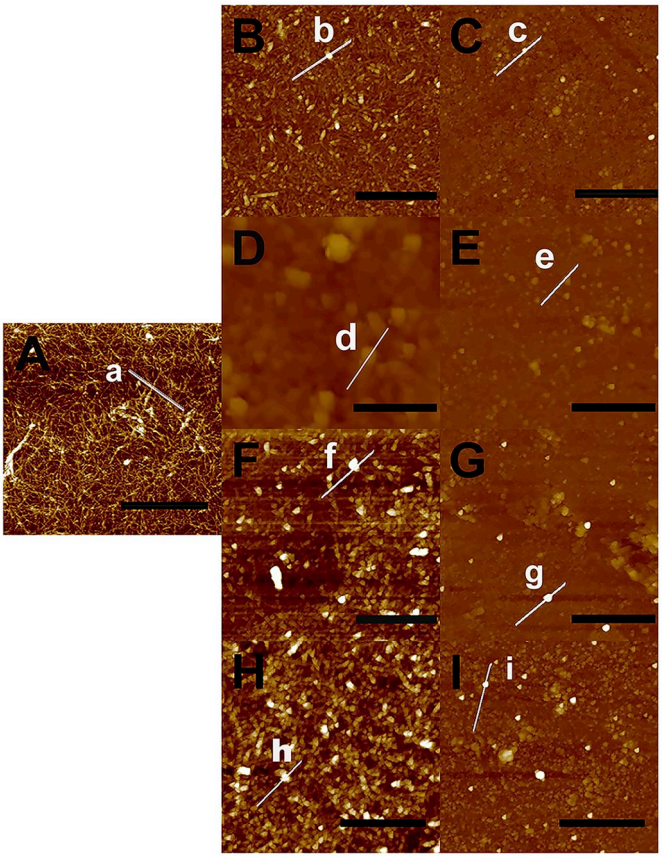

Fig. 2. AFM assay for the peptide aggregation images of 10 μM hIAPP19-37 in the presence of different concentration of complexes **1** (b,c), **2** (d,e), **3** (f,g), and **4** (h,i). The molar ratio of Au complex to hIAPP is 1 (b,d,f,h) and 10 (c,e,g,i) respectively. The scale bar is 2 μm.

current condition but disappeared when the molar ratio of compound to peptide increased to 10. For three other complexes, when the concentration of Au complexes increased to 10-fold excess, the spherical particles became much smaller and were less in quantity, thereby suggesting that the three complexes had a dramatic effect on

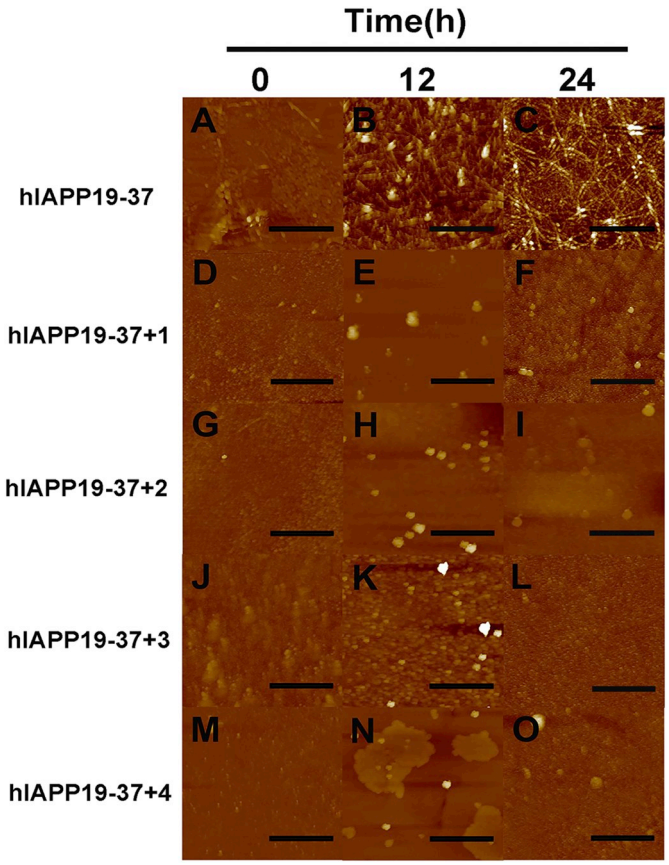

Fig. 3. AFM images of time-dependent aggregation of 10 μM hIAPP19-37 incubated with 100 μM Au complex for 0, 12 and 24 h at 310 K. The scale bar is 2 μm.

depolymerization of the fibrils. The height analysis is presented in Table S1, suggesting a remarkable particle size change in the AFM images. Fig. 3 exhibits the results of the time-dependent peptide aggregation. With time, the cultured peptide alone showed the development of some spherical particles and bushy fibers. Very sparse granular oligomers occurred in the images when complexes **1** and **2** were co-cultured with peptides. For the samples with complexes **3** and **4**, no fibers appeared, but some spherical particles were present.

These AFM results revealed that the Au complexes well inhibited and depolymerized the hIAPP19-37 aggregates. All of these complexes played notable roles in inhibiting the formation of peptide fibrils. The performances of complexes **3** and **4** were slightly inferior to those of **1** and **2**. These results were basically consistent with those of the ThT assay.

3.4. Particle size distribution

DLS is a sensitive tool used to detect the particle size distribution of peptide with or without Au complexes (Figs. 4 and S5). When hIAPP19-37 was incubated alone, the maximum particle size reached approximately 5600 nm. When the peptide was incubated in the presence of equivalent of Au complexes, the particles distributed around the 5600 nm almost vanished, as shown in Fig. 4. When 5-fold excess of complexes were added, the particle size was reduced to a small range, even to several nanometers. Fig. S5 presents the disaggregation results after the Au complexes were added to the aged peptide and further co-cultured. As the concentration of the complexes increased, the particle size of the aggregates decreased to a much smaller scale. The data demonstrated that the size distribution scope changed from micro to nanoscale in the presence of Au complexes, illustrating that the four Au complexes improved inhibition and depolymerization on hIAPP19-37 fibril formation.

3.5. Interactions of hIAPP19-37 with Au complexes

Intrinsic fluorescence quenching was applied to determine the apparent K_d of the interaction system by exciting the residue Tyr37 of hIAPP19-37. As expected, the fluorescence intensity decreased after the complex was added successively (Fig. 5). The apparent K_d values were 0.20 ± 0.008, 0.38 ± 0.021, 3.07 ± 0.24 and 3.66 ± 0.13 μM for complexes **1**, **2**, **3**, and **4**, respectively. The decreasing fluorescent intensity also reflected the peptide conformational change induced by Au complexes. With the addition of Au complex, the peak produced a slight red shift, which was due to the increase in polarity around the residue Tyr37 in hIAPP19-37 upon the binding of Au complex to the peptide [42,43]. These findings indicated the strong binding affinity between the peptide and the Au complexes.

In the study of ESI-MS, the peptide was incubated with the complexes at different concentration ratios to identify probable binding patterns between the peptide and complexes. The results are shown in Fig. S6. For the addition of complex **1** to the peptide, the peak of free hIAPP19-37 at 1932.83 (1+) was detected, consistent with previous reports. Moreover, the adduct peaks at 1137.93 (2+) and 2274.77 (1+) referred to the complex of [hIAPP19-37 + Au(DDTC)]. The peak at 1309.91 (2+) represented the adduct of [hIAPP19-37 + 2Au (DDTC)]. When complex **2** was added, the produced adduct peaks at 2129.81 (1+), 2306.78 (1+), and 2989.3 (1+) corresponded to the assignment of [hIAPP19-37 + Au], [hIAPP19-37 + Au(PDT)Cl], and [hIAPP19-37 + 3Au(PDT)], respectively. For complex **3**, the adduct peaks were at 1155.02 (2+), 2382.25 (1+), and 2688.03 (1+), which referred to [hIAPP19-37 + Au(Me_2bpy)], hIAPP19-37 + [Au (Me_2bpy)Cl_2], and [hIAPP + 2Au(Me_2bpy)], respectively. The results of complex **4** with hIAPP19-37 displayed the adduct peaks at 1143.24 (2+) and 1539.85 (2+), which were assigned to [hIAPP19-37 + Au $(DMSO)_2$] and [hIAPP19-37 + 2[Au(t-Bu_2bpy)Cl_2]], respectively (Table 1).

3.6. Membrane protection and oligomer reduction by Au complexes

Oligomers have the greatest toxicity and are the main factors leading to cell membrane rupture [39,44]. The deposition of amyloid peptide damages the β-cells' membrane [45–47]. In the current work, membrane leakage assay was used to explore the membrane damage caused by hIAPP19-37 and the membrane protection mitigated by Au complexes. As shown in Fig. 6, the rupture rate of cell membranes caused by peptide alone progressively increased and equilibrated after 7 h. With the addition of Au compounds, the rupture rate of cell membranes began to decrease. After the systems reached equilibrium, the four complexes reduced membrane rupture to approximately 54%, 49%, 44%, 41% by **1**, **2**, **3**, and **4** respectively. Complexes **3** and **4** performed well in cell membrane protection. Our study indicated that the Au compounds were involved in regulation on peptide aggregation, and the formation of oligomers were inhibited.

Some studies have illustrated that oligomers but not fibers possess the strongest toxicity [47–49]. To explore the changes of oligomer formation, we performed an immune assay using antibody A11, which is a type of hIAPP antibody that specifically binds to the peptide's oligomers [40,50,51]. Fig. 7 shows that A11 antibody was bound to the incubated hIAPP19-37 and exhibited the maximum absorption value, thereby suggesting the existence of numerous oligomers. However, addition of Au compounds reduced the absorption value remarkably. For complexes **3** and **4** at 100 μM, the absorption value decreased to 30% of the peptide itself. The data revealed that these complexes inhibited the formation of oligomers. As mentioned above, the complexes could bind to hIAPP19-37 and change the conformation of the peptide [49]. The ELISA data were consistent with that found in the membrane

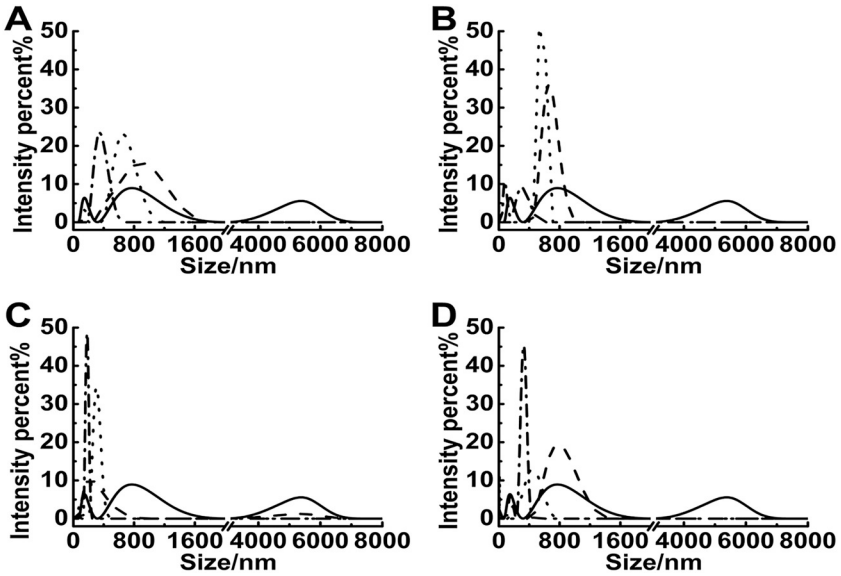

Fig. 4. DLS analysis of the multimodal size distribution of 10 μM hIAPP19-37 aggregates in the absence (solid) and presence of 1(dashed), 3(dotted), and 5 equivalents (dash dotted) of **1** (A), **2** (B), **3** (C), and **4** (D).

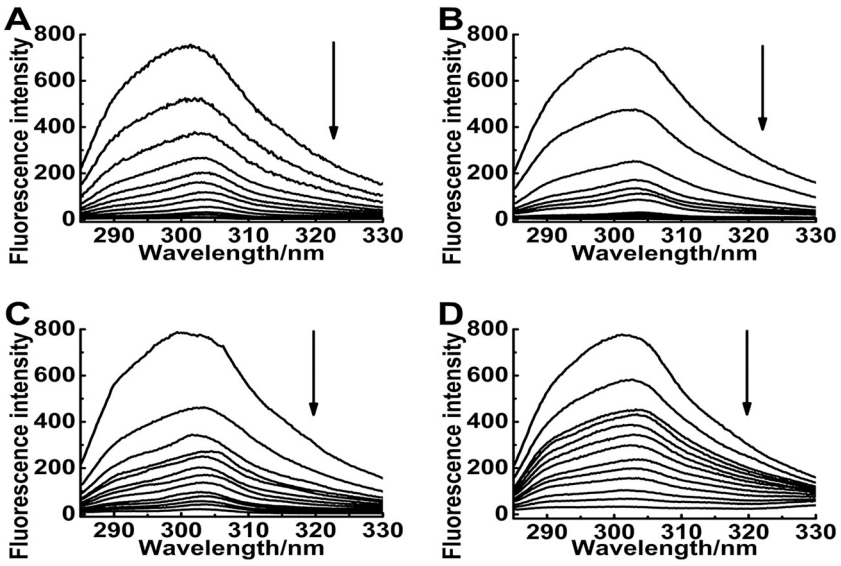

Fig. 5. Intrinsic fluorescence spectra of 10 μM hIAPP19-37 in the presence of Au complexes **1** (A), **2** (B), **3** (C) and **4** (D) at 298 K. The data were from the excitation of Tyr37 at 275 nm. The concentration of Au complex was 0, 0.2, 0.4, 0.6, 0.8, 1, 1.5, 2, 3, 4, 5, 7, and 10 μM, respectively (from top to bottom).

leakage observation.

3.7. Peptide-induced cytotoxicity affected by Au complexes

MTT assay was used to disclose the effects of amylin aggregation on cell viability and the regulation of Au complexes on peptide-induced cytotoxicity. Caffeic acid, an effective inhibitor of hIAPP, was used as a negative control in the experiments. In the absence of Au complexes, the incubated hIAPP19-37 reduced the cell viability to 43.3% ± 1.9% (Fig. 8). After incubation with 1.5 μM Au complexes, the cytotoxicity induced by the peptide was reduced as the cell viability increased to 61.7% ± 3.3%, 69.3% ± 2.4%, 70.7% ± 3.1%, and 74.7% ± 2.3% for Au complexes **1**, **2**, **3**, and **4**, respectively. When the concentration of Au complexes was increased to 15 μM, the cell viability was 47.4% ± 1.8%, 51.5% ± 2.6%, 54.3% ± 2.3%, and 57.2% ± 3.5% for complexes **1**, **2**, **3**, and **4**, respectively. The ANOVA analysis indicated that the metal complexes might have a good effect on the cell survival at low concentration. For the complexes themselves, they exhibited cytotoxicity to INS-1 rat cells at some extent (Fig. S7).

4. Discussion

The deposition of hIAPP is a vital factor correlated with T2DM, and the peptide aggregation to form fibers is attained through structural transformation. Peptide conformation after aggregation is distinct from the original state, and additional β-sheet components have been found [52]. Hence, inhibiting the aggregation and disassembling the aggregates of hIAPP may be a feasible way to manage T2DM. As a crucial part of hIAPP, the peptide hIAPP19-37 plays an important role in the deposition of full-length hIAPP. Some Au complexes produce good inhibitory effects on amyloid peptides, such as PrP106-126, hIAPP, and Aβ protein [29,53–56]. In this study, the four different molecules of Au compounds containing Au—S bonds or Au—N bonds were used to explore the interactions between them and hIAPP19-37, thereby revealing their inhibitory efficacy and disaggregation ability on hIAPP19-37 fibril formation.

Table 1
ESI-MS spectra of 50 μM hIAPP19-37 in the presence of Au complexes.

Complex	Calculated	Measured	Binding species
hIAPP19-37 + 1	1139.95(2+)	1137.93(2+)	hIAPP19-37 + Au(DDTC)
	1311.97(2+)	1309.91(2+)	hIAPP57 + 2Au(DDTC)
	1931.89(1+)	1932.83(1+)	hIAPP19-37
	2276.90(1+)	2274.77(1+)	hIAPP19-37 + Au(DDTC)
hIAPP19-37 + 2	1931.89(1+)	1932.28(1+)	hIAPP19-37
	2128.86(1+)	2129.81(1+)	hIAPP19-37 + Au
	2309.84(1+)	2306.78(1+)	hIAPP19-37 + Au(PDT)Cl
	2989.89(1+)	2989.30(1+)	hIAPP19-37 + 3Au(PDT)
hIAPP19-37 + 3	1156.49(2+)	1155.02(2+)	hIAPP19-37 + Au(Me_2bpy)
	1931.89(1+)	1931.73(1+)	hIAPP19-37
	2382.89(1+)	2382.25(1+)	hIAPP19-37 + [Au
	2691.13(1+)	2688.03(1+)	(Me_2bpy)Cl_2]
			hIAPP19-37 + 2Au(Me_2bpy)
hIAPP19-37 + 4	1142.31(2+)	1143.24(2+)	hIAPP19-37 + Au + 2DMSO
	1537.02(2+)	1539.85(2+)	hIAPP19-37 + 2[Au(t-
	1931.89(1+)	1932.09(1+)	Bu_2bpy)Cl_2]
			hIAPP19-37

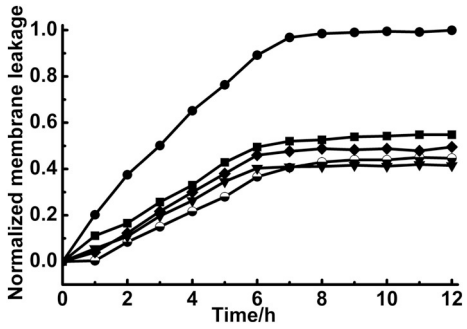

Fig. 6. hIAPP-induced membrane leakage in the absence (solid circle) and presence of Au complexes **1** (square), **2** (rhombus), **3** (triangle), and **4** (semi-solid circle). The concentrations of peptide and Au complex were 20 and 100 μM respectively.

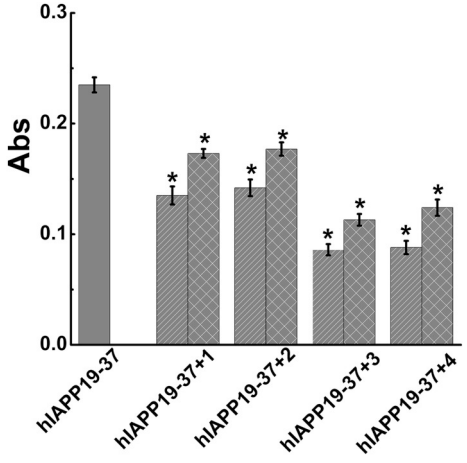

Fig. 7. ELISA assay of A-11 antibody with 100 μM hIAPP19-37 in the absence (solid) and presence of 100 (dense), 500 μM (sparse) of complexes **1**, **2**, **3** and **4** respectively. Data are shown as means ± SD, n = 3 in normal distribution. *p < 0.05 compared to the peptide by one-way ANOVA.

4.1. Effective inhibition of Au complexes on hIAPP aggregation

Although the self-aggregation ability of hIAPP19-37 was weaker than hIAPP1-37 [9], the fibrils were observed in our AFM images. As expected, peptide aggregation was reduced after incubation with Au complexes, especially with complexes **1** and **2**, as indicated by the ThT assay and AFM images. The morphological changes were intuitively

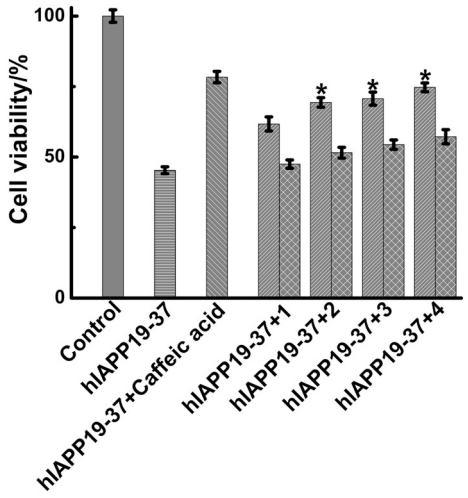

Fig. 8. Regulation of amyloid peptide-induced cytotoxicity by Au complexes. INS-1 cells were treated with 15 μM hIAPP19-37 (transverse stripes dense), hIAPP19-37 and 15 μM caffeic acid (medium), or hIAPP19-37 and different amounts of Au complexes at 1.5 (oblique stripe) and 15 μM (sparse). Cell viability was determined by MTT assay. Data represent the average of three experiments, *p < 0.05 compared to the peptide by one-way ANOVA.

observed by AFM, thereby eliminating the possible disturbance from ThT. The fibrils were decreased with a low dose of Au complexes and almost disappeared after being incubated with a high dose of Au complexes. The particle size of the aggregates decreased to nanoscale, as measured by DLS. The obtained inhibition and disaggregation data were in agreement with each other by the mentioned methods. The aggregation kinetics measured by AFM proved the inhibitory effects of Au complexes on peptide fibril formation. After comparing these data, we found that complex **2** had enhanced inhibitory effect on peptide aggregation, but combined with the cellular experiments, complexes **3** and **4** executed better effects than complex **2**.

4.2. Binding behaviors of Au complexes with hIAPP19-37

Au compounds interact with proteins and amyloid peptides mainly through metal coordination [55,57]. In our work, intrinsic fluorescence quenching and ESI-MS data were used to demonstrate the binding behaviors of these Au complexes with hIAPP19-37. Changes in the fluorescence quenching indicated the interactions of Au complexes with hIAPP19-37 and the peptide conformational change by the complexes. We also observed that Au complexes decreased the fluorescence of Tyr37, which might be caused by π–π stacking interaction when the complexes bound to the aromatic region of hIAPP19-37. The apparent dissociating constant was in micromolar grade, thereby indicating a strong interaction between them.

The ESI-MS data showed the possible binding mode of Au complexes with hIAPP19-37. We observed the adduct peak of peptide + Au[ligand] accompanying with the release of coordinated chloride atoms, indicating metal coordination contributed to the interaction between hIAPP19-37 and Au complexes. Interestingly, the adduct peak was also found in a mode of peptide + Au[ligand]Cl_2 in complexes **3** and **4**. As the Au[ligand]Cl_2 was charged positively, the binding might be attributed to the electrostatic interaction. Furthermore, hIAPP19-37 is a crucial hydrophobic fragment of hIAPP that contains some nonpolar residues. Interaction between the peptide and Au complex might be partly due to hydrophobic interaction [7,9,52], besides metal coordination and electrostatic interaction.

4.3. Roles of Au complexes in resisting oligomer formation

Peptide oligomers are a major factor in inducing cytotoxicity and

membrane leakage. Au complexes remarkably regulate the peptide-induced membrane leakage and improved the cell viability at some extent. Moreover, the immune assay using A11 antibody indicated that Au complexes effectively reduced oligomer formation as the antibody A11 specifically bound to the amylin oligomers. Complexes **3** and **4** performed better than complexes **1** and **2** relatively, which might be attributed to their lower self-cytotoxicity.

Au compounds have been widely used in the field of biomedicine, examples of which are auranofin in treating rheumatoid arthritis and nano Au materials used as drug carriers to cross the blood-brain barrier [18,53]. Au compounds may bind with various proteins and amyloid peptides due to good coordination ability of metal center. In our present work, two complexes with Au−S bonds and two complexes with Au−N bonds were used and compared. Among the four complexes, complexes **1** and **2** are of good binding affinity with hIAPP19-37, as mentioned above. Comparing those compounds by ThT assay, DLS measurement, and AFM images, the Au−S complexes exhibited relatively strong inhibition and disaggregation abilities. The ELISA assay, membrane leakage, and MTT analysis results suggested that the Au−N complexes well reduced the cytotoxicity caused by the peptides and oligomers. Complexes **3** and **4** may well inhibit the formation of oligomers in cellular environment, probably due to their specific molecular configuration and binding pattern. Although the present doses of Au compounds in cell culture conditions seem high compared to therapeutic conditions, based on the present fundamental study, we aim to find more favorable molecular configuration, modify current molecular structure, and design more effective inhibitors against amyloidosis in the future work.

4.4. hIAPP19-37 and hIAPP1-37

As mentioned above, the fragment hIAPP19-37 is a core fragment of the full-length of hIAPP1-37, which contains the crucial sequence 20-29 and can self–aggregate to form amyloid fibrils. By contrast, for the full-length hIAPP1-37, the existence of disulfide bond between cystine residues (Cys2-Cys7) stabilizes the helical structures spanning residues 5–17, and the residue His18 contributes to the turn formation around 18–21 when the peptide self-aggregates through β-sheet folding and assembly [6,15,58]. In the study of hIAPP and other amyloid peptides, such as Aβ and PrP106-126, it is known that the residue histidine offers a highly active site to bind with metal ions. In this work, we explored the binding mode between Au complexes and hIAPP19-37, and compared them with the full length of hIAPP1-37. Unexpectedly, the lack of His18 affected the binding mode of Au complexes with the peptide. The aggregation ability of hIAPP19-37 was also weaker than hIAPP1-37 in vitro as observed by AFM and ThT assay [9].

5. Conclusion

We studied the inhibition and depolymerization abilities of the Au complexes on hIAPP19-37. The four compounds well inhibited the peptide aggregation and scattered the aggregates into nanoscale particles. Complexes **1** and **2** had relatively better binding affinity with hIAPP19-37 and inhibitory effects on peptide aggregation than complexes **3** and **4**. They bind to the peptide mainly through metal coordination, hydrophobic interaction, and electrostatic interaction, as indicated by the experiment's results. Moreover, the Au complexes exhibited remarkable effects on the regulation of the peptide-induced cytotoxicity and reduction of oligomer formation. The Au−N complexes **3** and **4** demonstrated better cellular behaviors than complexes **1** and **2** due to the difference between the structures of Au−S and Au−N compounds. This work paves the way for the use of Au complexes as potential metallodrugs against amyloidosis-related disorders.

Abbreviations

Aβ	amyloid-β protein
T2DM	type 2 diabetes mellitus
hIAPP	human islet amyloid polypeptide
Phe	phenylalanine
Tyr	tyrosine
PrP	prion protein
ThT	thioflavin T
AFM	atomic force microscopy images
DLS	dynamic light scattering analysis
ESI-MS	electrospray ionization mass spectrometry
DDTC	dichloro diethyl dithiocarbamate
PDT	dichloro pyrrolidine dithiocarbamate
(Me)2bpy	4-4′-dimethyl-2,2′-bipyridyl
(t-Bu)2bpy	4-4-Di-tert-butyl-2,2′-bipyridyl
UV-Vis	ultraviolet–visible
DOPG	1, 2-dioleoyl-sn-glycero-3-phospho-rac-(1-glycerol) sodium salt
DOPC	1, 2-dioleoyl-sn-glycero-3-phosphocholine
MTT	3-(4, 5-dimethyl-2-thiazolyl)-2, 5-diphenyltetrazolium bromide
PBS	phosphate buffer saline
DMSO	dimethyl sulfoxide
LUVs	large unilamellar vesicles
ELISA	enzyme linked immunosorbent assay
BSA	bovine serum albumin
ANOVA	Analysis of Variance
INS-1 cells	Insulinoma beta cells in rat
Cys	Cystine

Acknowledgements

The project is supported by the National Natural Science Foundation of China, China (Nos. 21473251 & 21271185).

Appendix A. Supplementary data

Supplementary data to this article can be found online at https://doi.org/10.1016/j.jinorgbio.2019.110807.

References

[1] P.E.S. Smith, J.R. Brender, A. Ramamoorthy, J. Am. Chem. Soc. 131 (2009) 4470–4478.
[2] F. Chiti, C.M. Dobson, Annu. Rev. Biochem. 86 (2017) 27–68.
[3] B. Ren, Y. Liu, Y. Zhang, Y. Cai, X. Gong, Y. Chang, L. Xu, J. Zheng, ACS Chem. Neurosci. 9 (2018) 1215–1224.
[4] K. Weise, D. Radovan, A. Gohlke, N. Opitz, R. Winter, ChemBioChem 11 (2010) 1280–1290.
[5] A. Abedini, D.P. Raleigh, J. Mol. Biol. 355 (2006) 274–281.
[6] M. Wang, J. Yang, J. Wang, X. Wang, Chinese J. Chem. 30 (2012) 241–248.
[7] W. Du, G. Gong, W. Wang, J. Xu, J. Biol. Inorg. Chem. 22 (2017) 1065–1074.
[8] R. Kayed, J. Bernhagen, N. Greenfield, K. Sweimeh, H. Brunner, W. Voelter, A. Kapurniotu, J. Mol. Biol. 287 (1999) 781–796.
[9] J. Xu, B. Zhang, G. Gong, X. Huang, W. Du, J. Inorg. Biochem. 197 (2019) 110721–110730.
[10] L.M. Young, J.C. Saunders, R.A. Mahood, C.H. Revill, R.J. Foster, L.-H. Tu, D.P. Raleigh, S.E. Radford, A.E. Ashcroft, Nat. Chem. 7 (2014) 73–81.
[11] P. Patel, K. Parmar, V.K. Vyas, D. Patel, M. Das, J. Mol. Graph. Model. 77 (2017) 295–310.
[12] Y. Zou, Z. Qian, Y. Sun, G. Wei, Q. Zhang, J. Phys. Chem. B 121 (2017) 9203–9212.
[13] J.C. Dabrowiak, Inorg. Chim. Acta 393 (2012) 1–2.
[14] S. Dasari, P. Bernard Tchounwou, Eur. J. Pharmacol. 740 (2014) 364–378.
[15] J.R. Brender, K. Hartman, R.P.R. Nanga, N. Popovych, R. de la Salud Bea, S. Vivekanandan, E.N.G. Marsh, A. Ramamoorthy, J. Am. Chem. Soc. 132 (2010) 8973–8983.
[16] E.C. Long, J. Am. Chem. Soc. 131 (2009) 14124–14125.
[17] D. Hu, H. Xu, B. Xiao, D. Li, Z. Zhou, X. Liu, J. Tang, Y. Shen, ACS Appl. Mater. Inter. 10 (2018) 34974–34982. American Chemical Society.
[18] J.M. Madeira, D.L. Gibson, W.F. Kean, A. Klegeris, Inflammopharmacology 20 (2012) 297–306.

[19] V. Milacic, D. Fregona, Q.P. Dou, Histol. Histopathol. 23 (2008) 101–108.
[20] H. Li, E. Ha, R.P. Donaldson, A.M. Jeremic, A. Vertes, Anal. Chem. 87 (2015) 9829–9837.
[21] L. He, X. Wang, C. Zhao, H. Wang, W. Du, Metallomics 5 (2013) 1599–1603.
[22] G. Gong, W. Wang, W. Du, RSC Adv. 7 (2017) 18512–18522.
[23] T.P. Shareena Dasari, Y. Zhang, H. Yu, Biochem. Pharmacol. 4 (2015).
[24] T. Zou, C.T. Lum, C.-N. Lok, J.-J. Zhang, C.-M. Che, Chem. Soc. Rev. 44 (2015) 8786–8801.
[25] C.-M. Che, R.W.-Y. Sun, Chem. Commun. 47 (2011) 9554–9560.
[26] G. Ferraro, C. Gabbiani, A. Merlino, Bioconjug. Chem. 27 (2016) 1584–1587.
[27] S. Neupane, Y. Pan, H. Li, K. Patnode, J. Farmakes, G. Liu, Z. Yang, ACS Appl. Nano Mater. 1 (2018) 4053–4063.
[28] W. Wei, Y. Sun, M. Zhu, X. Liu, P. Sun, F. Wang, Q. Gui, W. Meng, Y. Cao, J. Zhao, J. Am. Chem. Soc. 137 (2015) 15358–15361.
[29] L. He, D. Zhu, C. Zhao, X. Jia, X. Wang, W. Du, J. Inorg. Biochem. 152 (2015) 114–122.
[30] G. Marcon, S. Carotti, M. Coronnello, L. Messori, E. Mini, P. Orioli, T. Mazzei, M.A. Cinellu, G. Minghetti, J. Med. Chem. 45 (2002) 1672–1677.
[31] A. Casini, M.C. Diawara, R. Scopelliti, S.M. Zakeeruddin, M. Grätzel, P.J. Dyson, Dalton T. 39 (2010) 2239–2245.
[32] A.P. Martins, A. Ciancetta, A. de Almeida, A. Marrone, N. Re, G. Soveral, A. Casini, ChemMedChem 8 (2013) 1086–1092.
[33] V. Amani, A. Abedi, S. Ghabeshi, H.R. Khavasi, S.M. Hosseini, N. Safari, Polyhedron 79 (2014) 104–115.
[34] R.T. Mertens, J.H. Kim, W.C. Jennings, S. Parkin, S.G. Awuah, Dalton T. 48 (2019) 2093–2099.
[35] L. Ronconi, L. Giovagnini, C. Marzano, F. Bettìo, R. Graziani, G. Pilloni, D. Fregona, Inorg. Chem. 44 (2005) 1867–1881.
[36] J. Cordón, G. Jiménez-Osés, J.M. López-de-Luzuriaga, M. Monge, M.E. Olmos, D. Pascual, Organometallics 33 (2014) 3823–3830.
[37] M.A. Ivanov, M.V. Puzyk, T.A. Tkacheva, K.P. Balashev, Russ. J. Gen. Chem. 73 (2003) 1821–1822.
[38] A. Sgarbossa, F. Lenci, J. Fluoresc. 23 (2013) 561–567.
[39] J.R. Brender, E.L. Lee, M.A. Cavitt, A. Gafni, D.G. Steel, A. Ramamoorthy, J. Am. Chem. Soc. 130 (2008) 6424–6429.
[40] R. Kayed, E. Head, J.L. Thompson, T.M. McIntire, S.C. Milton, C.W. Cotman, C.G. Glabe, Science 300 (2003) 486.
[41] H. LeVine, Method. Enzymol. 309 (1999) 274–284.
[42] T.I. Chandel, A. Masroor, M.K. Siddiqi, I.A. Siddique, I. Jahan, M. Ali, S.M. Nayeem, V.N. Uversky, R.H. Khan, J. Mol. Liq. 278 (2019) 553–567.
[43] P. Bolel, S. Datta, N. Mahapatra, M. Halder, J. Phys. Chem. B 116 (2012) 10195–10204.
[44] E. Sparr, M.F. Engel, D.V. Sakharov, M. Sprong, J. Jacobs, B. de Kruijff, J.W. Hoppener, J.A. Killian, FEBS Lett. 577 (2004) 117–120.
[45] G. Pappalardo, D. Milardi, A. Magri, F. Attanasio, G. Impellizzeri, C. La Rosa, D. Grasso, E. Rizzarelli, Chemistry 13 (2007) 10204–10215.
[46] D.L. Heyl, J.M. Osborne, S. Pamarthy, S. Samisetti, A.W. Gray, A. Jayaprakash, S. Konda, D.J. Brown, S.R. Miller, R. Eizadkhah, M.C. Milletti, Int. J. Pept. Res. Ther. 16 (2010) 43–54.
[47] L. Khemtemourian, J.A. Killian, J.W.M. Hoppener, M.F.M. Engel, Exp. Diabetes Res. (2008) (2008) 421287–421295.
[48] L. Haataja, T. Gurlo, C.J. Huang, P.C. Butler, Endocr. Rev. 29 (2008) 303–316.
[49] A. Laganowsky, C. Liu, M.R. Sawaya, J.P. Whitelegge, J. Park, M. Zhao, A. Pensalfini, A.B. Soriaga, M. Landau, P.K. Teng, D. Cascio, C. Glabe, D. Eisenberg, Science 335 (2012) 1228–1231.
[50] M.F. Tomasello, A. Sinopoli, F. Attanasio, M.L. Giuffrida, T. Campagna, D. Milardi, G. Pappalardo, Eur. J. Med. Chem. 81 (2014) 442–455.
[51] J.J. Meier, R. Kayed, C.Y. Lin, T. Gurlo, L. Haataja, S. Jayasinghe, R. Langen, C.G. Glabe, P.C. Butler, American journal of physiology. Endocrinol. Metab. 291 (2006) 1317–1324.
[52] L. He, X. Wang, C. Zhao, D. Zhu, W. Du, Metallomics 6 (2014) 1087–1096.
[53] Q. Ma, G. Wei, X. Yang, Nanoscale 5 (2013) 10397–10403.
[54] M. Song, Y. Sun, Y. Luo, Y. Zhu, Y. Liu, H. Li, Int. J. Mol. Sci. 19 (2018) 1815–1821.
[55] W. Wang, C. Zhao, D. Zhu, G. Gong, W. Du, J. Inorg. Biochem. 171 (2017) 1–9.
[56] C. Zhao, X. Wang, L. He, D. Zhu, B. Wang, W. Du, Metallomics 6 (2014) 2117–2125.
[57] L.A. Levchenko, A.P. Sadkov, N.V. Lariontseva, V.S. Kulikova, A.K. Shilova, A.E. Shilov, Dokl. Biochem. Biophys. 394 (2004) 33–34.
[58] R. Laghaei, N. Mousseau, G. Wei, J. Phys. Chem. B 114 (2010) 7071–7077.